Published in final edited form as:
NMR Biomed. 2012 November ; 25(11): 1234–1244. doi:10.1002/nbm.2794.

Metabolism of [U-^{13}C]glucose in Human Brain Tumors *In Vivo*

Elizabeth A. Maher[1,2,3,4,*], **Isaac Marin-Valencia**[2,5], **Robert M. Bachoo**[1,2,3,4], **Tomoyuki Mashimo**[1,3,4], **Jack Raisanen**[4,7], **Kimmo J. Hatanpaa**[4,7], **Ashish Jindal**[6], **F. Mark Jeffrey**[6], **Changho Choi**[6], **Christopher Madden**[4,8], **Dana Mathews**[9], **Juan M. Pascual**[2,5,10], **Bruce E. Mickey**[4,8], **Craig R. Malloy**[1,6,11], and **Ralph J. DeBerardinis**[3,5,12,*]

[1]Department of Internal Medicine, University of Texas Southwestern Medical Center, Dallas

[2]Department of Neurology, University of Texas Southwestern Medical Center, Dallas

[3]Harold C. Simmons Comprehensive Cancer Center, University of Texas Southwestern Medical Center, Dallas

[4]Annette G. Strauss Center for Neuro-Oncology, University of Texas Southwestern Medical Center, Dallas

[5]Department of Pediatrics, University of Texas Southwestern Medical Center, Dallas

[6]Advanced Imaging Research Center, University of Texas Southwestern Medical Center, Dallas

[7]Department of Pathology, University of Texas Southwestern Medical Center, Dallas

[8]Department of Neurological Surgery, University of Texas Southwestern Medical Center, Dallas

[9]Department of Radiology, University of Texas Southwestern Medical Center, Dallas

[10]Department of Physiology, University of Texas Southwestern Medical Center, Dallas

[11]Medical Service, Veterans Affairs North Texas Healthcare System, Lancaster, Texas 75216

[12]McDermott Center for Human Growth and Development, University of Texas Southwestern Medical Center, Dallas, Texas 75390

Abstract

Glioblastomas (GBMs) and brain metastases demonstrate avid uptake of ^{18}fluoro-2-deoxyglucose (FDG) by positron emission tomography (PET) and display perturbations of intracellular metabolite pools by ^{1}H magnetic resonance spectroscopy (MRS). These observations suggest that metabolic reprogramming contributes to brain tumor growth *in vivo*. The Warburg effect, excess metabolism of glucose to lactate in the presence of oxygen, is a hallmark of cancer cells in culture. FDG-positive tumors are assumed to metabolize glucose in a similar manner, with high rates of lactate formation compared to mitochondrial glucose oxidation, but few studies have specifically examined the metabolic fates of glucose *in vivo*. In particular, the capacity of human brain malignancies to oxidize glucose in the tricarboxylic acid cycle is unknown. Here we studied the metabolism of human brain tumors *in situ*. [U-^{13}C]glucose was infused during surgical resection, and tumor samples were subsequently subjected to ^{13}C NMR spectroscopy. Analysis of tumor metabolites revealed lactate production, as expected. We also determined that pyruvate dehydrogenase, turnover of the TCA cycle, anaplerosis and *de novo* glutamine and glycine synthesis contributed significantly to the ultimate disposition of glucose carbon. Surprisingly, less than 50% of the acetyl-CoA pool was derived from blood-borne glucose, suggesting that

Corresponding authors: Elizabeth A. Maher, MD, PhD, 5323 Harry Hines Blvd, Dallas, TX 75390-9186, 214-645-5905 (phone), 214-645-5999 (fax), elizabeth.maher@utsouthwestern.edu, Ralph J. DeBerardinis, MD, PhD, 5323 Harry Hines Blvd, Room K4.216, Dallas, TX 75390-8502, 214-648-5402 (phone), 214-648-2096 (fax), ralph.deberardinis@utsouthwestern.edu.

additional substrates contribute to tumor bioenergetics. This study illustrates a convenient approach that capitalizes on the high information content of ^{13}C NMR spectroscopy and enables the analysis of intermediary metabolism in diverse malignancies growing in their native microenvironment.

Keywords

Cancer; glioblastoma; metabolism; Warburg effect; glucose; glutamine; NMR

INTRODUCTION

Reprogramming of energy metabolism is considered to be a hallmark of malignant transformation [1]. This concept has roots in the 1920s when Warburg demonstrated that tumors, relative to normal tissues, display excess glycolysis and lactate production in the presence of oxygen (the “Warburg effect”) [2, 3]. This observation led to a model that has dominated the study of cancer metabolism for most of the last 80 years: that malignant transformation shifts glucose metabolism away from efficient energy-producing pathways in the mitochondria towards glycolysis as the major source of energy [4]. Warburg’s work foreshadowed the clinical practice of monitoring glucose uptake in tumors with a glucose analogue, 2-^{18}fluoro-2-deoxyglucose (^{18}FDG), and imaging by positron emission tomography (PET). This procedure exploits the tumor's ability to transport glucose more rapidly than surrounding tissue. The mechanisms that drive enhanced glucose metabolism in tumors, and the benefits of this metabolic phenomenon at the cellular level, are complex and incompletely understood. Expression of glucose transporters and glycolytic enzymes is driven by oncogenes and hypoxia-inducible factor-1 (HIF-1) in cancer cell lines and possibly *in vivo* [5–7]. In a minority of tumors, mutations that overtly impair oxidative metabolism probably also stimulate glycolysis during tumor growth [8–11]. Furthermore, evidence from experimental models suggests that excess glucose metabolism actually confers superior cell growth by maintaining pools of essential glycolytic intermediates and other effector molecules [5, 12–15].

However, despite the widespread use of ^{18}FDG-PET as a surrogate for tumor glycolysis [16], no information beyond glucose uptake can be gleaned from these scans, making it difficult to design rational therapeutic strategies aimed at interfering with tumor energy formation. In ^{18}FDG-PET-avid tumors, it is not known whether glucose is metabolized exclusively to pyruvate and lactate, or whether glucose carbons can be oxidized in the TCA cycle. Entry of glucose carbons into the cycle would also provide macromolecular precursors (e.g. citrate, succinyl-CoA, nonessential amino acids, nucleotides, fatty acids) necessary for tumor growth [17–19]. Stable isotope tracers such as ^{13}C-enriched glucose are valuable tools to probe metabolism *in vivo*, because the distribution of ^{13}C in metabolites downstream of glucose, analyzed by ^{13}C nuclear magnetic resonance (NMR) spectroscopy, provides a wealth of information about metabolism in the tissue of interest. Because these tracers are not radioactive, they can safely be infused into human patients in sufficient quantities to significantly enrich informative metabolites. Although real-time acquisition of ^{13}C spectra from live patients is potentially useful [20], limited spatial resolution and partial volume effects of *in vivo* ^{13}C NMR spectroscopy restrict its practicality for cancer. Alternatively, extracts of surgically-resected tissues obtained from subjects infused with ^{13}C-glucose can be analyzed *ex vivo* [21, 22]. This approach is feasible when surgical resection of the primary tumor is planned in the course of treatment.

The urgent need for novel therapeutics in malignant gliomas stems from their rapid progression and lethality despite aggressive multimodality therapy. Glioblastomas (GBMs)

and brain metastases demonstrate avid ^{18}FDG uptake by PET, often exceeding the high rate of glucose uptake in the normal cortex, and display marked perturbations of intracellular metabolite pools by ^{1}H magnetic resonance spectroscopy (MRS) [23–25]. These findings suggest that metabolic reprogramming contributes to GBM growth and may be a useful therapeutic target. In the current study, we optimized a [U-^{13}C]glucose infusion protocol that produced high-quality proton-decoupled ^{13}C NMR spectra from metabolites extracted from nine primary high-grade gliomas and two metastatic brain tumors. In each tumor, glucose was oxidized in the TCA cycle and was used to produce macromolecular precursors, reflecting a complex metabolic phenotype that included, but was not limited to, the conversion of glucose to lactate. A significant fraction of the acetyl-CoA used in the TCA cycle was not derived from blood-borne glucose, suggesting that additional substrates besides glucose also provide energy during brain tumor growth.

MATERIALS AND METHODS

Clinical Protocol

Patients were enrolled in an IRB-approved clinical protocol after obtaining informed consent. Nine patients were selected for inclusion on the basis of an MR scan consistent with a high grade glioma. Two additional patients were selected on the basis of a histologically verified extra-cranial malignancy (breast, lung) and an MR scan revealing a solitary brain metastasis. ^{18}FDG-PET scans were performed prior to the day of surgical resection. On the morning of surgery, the patients had a peripheral intravenous line placed, and sterile, pyrogen-free [U-^{13}C]glucose (Cambridge Isotope Laboratories) was infused at 4g/hr (patients 1–3), or as a bolus of 8g over 10 minutes followed by 8g/hr continuous infusion (patients 4–11). Standard procedures were followed for the craniotomy and removal of the tumor. For metabolic analysis, an effort was made to select tumor samples composed as completely as possible of viable neoplastic cells. These were identified from the region of tumor that enhanced most evenly on a pre-operative MR scan, correlated with avid ^{18}FDG glucose uptake, and/or was identified intraoperatively using fixed anatomic landmarks or surgical navigation (VectorVision, Brainlab Inc, Westchester, IL). A portion of each specimen submitted for metabolic analysis was examined histologically for diagnostic purposes and to estimate tumor cellularity. Immediately upon removal, each tumor fragment was immersed in iced saline, gently washed to remove blood and adherent tissue, and split for pathological examination and for NMR analysis. The mass of samples for NMR ranged from 150 – 400 mg. The total time between removal of each fragment from the patient and freeze-clamping was approximately 1 minute. All diagnoses were made by a clinical pathologist. DNA sequencing revealed that none of these tumors had mutations in isocitrate dehydrogenase isoforms 1 or 2 (*IDH1* or *IDH2*).

Mass spectrometry

Blood was obtained prior to infusion of [U-^{13}C]glucose and approximately every 30 minutes during the infusion until the end of tumor sampling. Blood was drawn from an arterial line or from a venous site in the contralateral arm. Samples were centrifuged to separate the plasma and frozen in liquid nitrogen. A 10μL aliquot was vortexed with 40μL of water and extracted in equal volumes of chloroform, methanol and water. The aqueous phase was re-extracted with chloroform, evaporated, derivatized in 100μL of a trimethylsilyl donor (TriSil, Pierce), and analyzed using an Agilent 6890 gas chromatograph coupled to an Agilent 5973N Mass Selective Detector. Glucose enrichment was determined by comparing the ratio of fragment ions 206 and 441 (enriched) and 204 and 435 (unenriched) to a standard curve. To determine ^{13}C enrichment in lactate and glutamine, the measured distribution of mass isotopomers was corrected for natural abundance [26].

Tissue Processing and NMR Spectroscopy

Frozen tumor samples were powdered in a mortar under liquid nitrogen with 4% perchloric acid (1:4 w/v), thawed, and centrifuged at 47,800 *g* for 15 min. The supernatant was transferred to a new tube, where chloroform/tri-n-octylamine (78%/22%; v/v) was added in a 1:2 volumetric ratio to increase the pH to ~6. The samples were centrifuged at 3,300 *g* for 15 min. The aqueous phase was removed and transferred to a microfuge tube, lyophilized and reconstituted in 200μL deuterium oxide (Cambridge Isotope Laboratories). The pH was adjusted to 7.0 with 2–3μL of 1M sodium deuteroxide (Cambridge Isotope Laboratories) followed by centrifugation at 18,400 *g* for 1 min. The supernatant was transferred to a 3-mm NMR tube for NMR analysis. Proton-decoupled ^{13}C NMR spectra of tumor extracts were acquired by a Varian VNMRS Direct Drive 14.1T 600 MHz vertical bore system (Agilent) with a 3 mm probe. Shimming was performed on ^{2}H signal from the solvent $^{2}H_2O$, and a field-frequency lock was used. Acquisition conditions included: flip angle, 45 degrees; bandwidth 34,965 Hz acquired into 104,986 points; acquisition time, 1.5 seconds; delay, 4.5 second delay; proton decoupling with WALTZ - 16. Typically 8,000 to 10,000 scans were acquired. The ^{13}C free induction decay was processed and analyzed using Advanced Chemistry Development software. After baseline correction, data were zero-filled twice and multiplied by a 0.5 – 0.8 Hz exponential prior to Fourier transformation. Each peak was fitted with a Gauss-Lorentz function and the area was measured for all peaks within informative multiplets. ^{13}C NMR spectra and glutamate isotopomers were analyzed as described previously using steady-state [27] and non steady-state analyses [28].

RESULTS

Glycolysis, glycine synthesis, and glucose oxidation in human GBMs

[U-^{13}C]glucose was infused at 4g/hr during initial surgical resection of untreated tumors in three GBM patients (patients 1–3, see Supporting Information Fig. S1). A representative case (patient 3) is shown in Fig. 1. A gadolinium-enhancing right temporoparietal mass with cystic and solid components (Fig. 1a) displayed avid uptake of ^{18}FDG at the tumor margins (Fig. 1b). ^{13}C-glucose enrichment in the plasma gradually increased during the infusion to a maximum of 25% at the time of tumor sampling (Fig. 1c). Mass spectrometry revealed that essentially all of the plasma glucose was either unlabeled or labeled in all six positions, with only a small fraction (3±2% for all patients in the study) containing one to five ^{13}C atoms. Thus essentially all of the labeled glucose entering the tumor was [U-^{13}C]glucose. Despite the relatively low enrichment in plasma glucose, ^{13}C–^{13}C spin-spin coupling was detected in many tumor metabolites (Fig. 1d). Coupling reflects adjacent ^{13}C nuclei arising from the metabolism of [U-^{13}C]glucose. ^{13}C–^{13}C coupling was observed in lactate and alanine, as expected for a high rate of glucose metabolism to pyruvate in glycolytic cells. ^{13}C–^{13}C coupling was also detected in glycine, an intermediate in nucleotide and protein synthesis recently identified as an important fate of glucose carbon in some tumor cells [29, 30]. The signal in lactate carbon 2 (LAC2) showed a large doublet of doublets, reflecting labeling at all three lactate carbons. The LAC2 multiplet also contained small 2–3 and 1–2 doublets, demonstrating that not all of the lactate in the tumor was uniformly labeled. These patterns arise from entry of glucose carbon into the TCA cycle followed by metabolism to pyruvate (pyruvate cycling) and lactate [31].

Unexpectedly, glutamate and glutamine were also labeled in all carbons analyzed in each GBM. The 4–5 doublet in glutamate and glutamine carbon 4 is derived from [1,2-^{13}C]acetyl-CoA produced from [U-^{13}C]glucose, demonstrating that glucose was metabolized to acetyl-CoA via pyruvate dehydrogenase (PDH). Labeling in glutamate carbon 2 and glutamate carbon 3 is consistent with turnover of the TCA cycle. The labeling patterns in glutamate and glutamine were similar at each carbon, demonstrating that

glutamate was converted to glutamine by the enzyme glutamine synthetase (GS). However, a complete quantitative isotopomer analysis was not possible because of the poor resolution of some of the multiplets, particularly the doublet of doublets in glutamate carbon 4 (Fig. 1d). A qualitative summary of metabolic activities observed in these GBMs is presented in Fig. 2.

Because cysts are common features of GBM, we also analyzed fluid from this patient's cyst. It contained abundant lactate (15.7 mM) compared to normal plasma levels (1–2 mM), and the ^{13}C NMR spectrum was dominated by lactate signals (Fig. 1e). Although small multiplets were present in the cyst lactate, unlike the tumor lactate, these multiplets were dwarfed by large singlets. Analysis by mass spectrometry revealed that less than 5% of the cyst lactate contained ^{13}C. Thus the singlets were due to naturally-occurring ^{13}C (1.1% of all carbon), rather than to lactate derived from ^{13}C-glucose, and entry of new glucose-derived lactate into the cyst did not occur rapidly enough to label a high fraction of this large pool. Like the plasma, the cyst fluid contained abundant glutamine (0.7 mM) and very little glutamate. Lack of ^{13}C–^{13}C multiplets in glutamine (Fig. 1e) revealed that tumor-derived glutamine was not secreted into the cyst over the time course of the infusion.

Production of acetyl-CoA from glucose and other fuels in GBM

We next tested the effects of higher enrichment in plasma glucose by infusing an initial bolus of 8g [U-^{13}C]glucose over 10 minutes followed by a continuous infusion of 8g/hr. One patient with a Grade III astrocytoma (patient 4, Fig. 3) and five untreated GBM patients with ^{18}FDG-positive masses (patients 5–9) were studied using this protocol. As anticipated, the patients displayed a rapid rise in ^{13}C labeling of plasma glucose, a 2–3 fold increase in final enrichment (typically exceeding 50%), and a long period of high enrichment in the plasma prior to tumor sampling (Fig. S1). In all cases, tumor specimens were collected after at least 100 minutes of the infusion (Fig. S1). In four normoglycemic patients, the final plasma enrichment was 49 – 65% and in one patient with steroid-induced hyperglycemia (patient 5), the enrichment was 32% (Table 1). Other circulating nutrients were only marginally labeled over the time course. Small amounts of uniformly-labeled lactate (9 ± 5% of the total plasma lactate pool) and glutamine with two additional mass units from ^{13}C (4 ± 3% of the total plasma glutamine pool) were detected by mass spectrometry at the end of these infusions.

The higher infusion rate improved the signal-to-noise in the NMR spectra, as illustrated in the Grade III astrocytoma patient (patient 4, Fig. 3d). Even in the hyperglycemic patient with the lowest plasma glucose enrichment, there was excellent resolution of ^{13}C multiplets (patient 5, Fig. 4e). ^{13}C–^{13}C coupling was observed in lactate and alanine in all tumors, and in glycine in 7 of the 8 GBM patients on either infusion protocol. Doublets were visible in LAC2, confirming pyruvate cycling in all of these tumors. The 4–5 doublets in glutamate and glutamine confirmed that PDH was active in all tumors. The doublet of doublets at GLU4 and GLN4 was also observed in all tumors. This multiplet demonstrates complete turnover of the TCA cycle because it can only occur if both acetyl-CoA and oxaloacetate are enriched in ^{13}C. All signals within the GLU2, GLU3 and GLU4 multiplets were resolved well enough to integrate peak areas with high confidence, so it was possible to perform a complete analysis of glutamate isotopomers to determine enrichments and relative fluxes related to core pathways of glucose metabolism [32]. Because we could not determine conclusively whether metabolic steady-state was established within the tumor, we applied both steady-state (SS) and non-steady-state (NSS) models (Table 1). We first determined the fractional enrichment in the acetyl-CoA pool (Fc3). In both models, a significant percentage of acetyl-CoA was labeled as [1,2-^{13}C]acetyl-CoA in the tumor (15±7% in the NSS model and 11±6% in the SS model). Acetyl-CoA enrichment was positively correlated with plasma glucose enrichment (Fig. 5). Surprisingly, however, in every tumor analyzed, the ^{13}C

enrichment in acetyl-CoA was much lower than the glucose enrichment in the plasma (Table 1). A nonsteady-state analysis was then used in two of the tumors subjected to the 4g/hr infusion. Again, although these tumors contained [1,2-^{13}C]acetyl-CoA, the measured fractional enrichment in acetyl-CoA was far lower than the plasma glucose enrichment (Table 1). These data suggest that other nutrients in addition to glucose were metabolized to acetyl-CoA and then oxidized in the TCA cycle to a significant degree in these tumors.

Anaplerosis is active in GBM

In addition to its role in efficient energy production, the TCA cycle plays a separate and equally essential role in biosynthesis and cell growth, because precursors for numerous macromolecules are produced in the TCA cycle. Anaplerosis is the process of replenishing TCA cycle intermediates that have been removed from the cycle for synthesis of macromolecules or neurotransmitters [17]. As measured by ^{13}C NMR isotopomer analysis, the anaplerotic flux in every tumor approached or exceeded entry of carbon into the TCA cycle via citrate synthase, with a total anaplerotic flux of 1.25 ± 0.43 (mean and SD) relative to citrate synthase for the five GBMs infused at 8g/hr (Table 1), indicating robust anaplerosis in these tumors.

Glucose oxidation in brain metastases

Taken together, these observations in high-grade gliomas demonstrate allocation of glucose carbon into multiple bioenergetic and biosynthetic pathways. It was unclear whether these properties are unique to these aggressive primary brain tumors or more broadly characterize tumors growing in the brain microenvironment. To address this question we studied two additional patients with systemic cancer (breast and non-small cell lung primaries) who had developed solitary metastases to the brain. The ^{13}C NMR spectra from the breast metastasis (Fig. 6) and lung metastasis (Fig. 7) shared many of the features observed in the GBMs, including ^{13}C–^{13}C multiplets in lactate, alanine, glutamate and glutamine. The breast metastasis also produced glycine from glucose (Fig. 6d, multiplet #7). Both tumors had prominent 4–5 doublets in GLU4, reflecting PDH flux. Steady-state modeling again revealed significant anaplerosis and enrichment in acetyl-CoA that was much lower than blood glucose (Table 1). Although limited to 2 patients, these cases represent two distinct cancer subtypes, and the metabolic similarity to primary brain tumors is striking.

DISCUSSION

Three advances are presented in this work. First, we used ^{13}C-glucose to probe the metabolism of human gliomas and brain metastases *in situ*. This produced a novel and biologically relevant view of glucose metabolism in these tumors, a significant step forward from previous metabolic studies relying exclusively on cancer cell lines cultured in glucose excess and otherwise non-physiological conditions. Second, glucose and other fuels were oxidized in the TCA cycle of these tumors, indicating that energy production involves numerous pathways in addition to the Warburg effect. Third, the metabolism of eleven individual tumors was remarkably similar, suggesting that it is a common feature of aggressive tumor growth in the brain rather than the effect of a specific mutation or histological type.

^{13}C-enriched glucose and detection of ^{13}C-enriched products by NMR has been applied in earlier studies of tumor metabolism using the rat C6 glioma model. This malignancy was induced in rats by exposure to N,N'-nitroso-methylurea, and tumor cells can either be cultured *ex vivo* or re-implanted into new hosts, producing tumors with morphological similarities to glioblastoma multiforme [33]. In some respects, results from the C6 model are consistent with the current report. Bouzier and colleagues, for example, found

significant ^{13}C enrichment in glutamate, glutamine, GABA and aspartate from perchloric acid extracts of C6 gliomas resected after a 60 min infusion of [1-^{13}C]glucose [34]. Although it was not mentioned in this report, the published ^{13}C spectra appear to show ^{13}C – ^{13}C spin-spin coupling in glutamate, exactly as would be anticipated if a significant fraction of acetyl-CoA entering the TCA cycle was derived from [1-^{13}C]glucose, as reported here for human tumors. However, other reports, also using [1-^{13}C]glucose in the same C6 model, reached the opposite conclusion [35]. Even after prolonged infusion, enrichment of glutamate carbons 3 and 4 was readily detected in normal brain but not in the tumor. For this reason, the mathematical analysis of glucose metabolism in that report rested on the assumption that oxidation in the TCA cycle was negligible.

The ^{13}C labeling pattern in glucose, [U-^{13}C]glucose, was chosen over alternatives because the intent was to achieve maximal enrichment of the pyruvate pool to increase the likelihood of detecting flux through PDH. This labeling pattern eliminates the ambiguity associated with labeling patterns producing singly-labeled acetyl-CoA, such as [1-^{13}C]glucose or [1,6-^{13}C]glucose, because the resulting singlets in glutamate can be difficult to distinguish from natural abundance ^{13}C if turnover of the TCA cycle is slow. Although [1,2-^{13}C]glucose is preferable to detect activity of the oxidative pentose phosphate shunt, only half of the pyruvate produced from [1,2-^{13}C]glucose contains ^{13}C. Furthermore, from a practical perspective, [U-^{13}C]glucose is relatively inexpensive, greatly improving the affordability of human experiments involving steady-state infusions. We focused on ^{13}C NMR spectroscopy since the information encoded in spin-spin coupling makes this the single most powerful technique to analyze complex metabolic pathways from individual samples. Crucially, the infusions with ^{13}C enabled us to analyze the relative activities of metabolic pathways as opposed to simply measuring metabolite abundance.

Because the sensitivity of ^{13}C NMR is low, the choice of infusion parameters was essential to obtain spectra of the highest quality. Using a bolus and an infusion rate of 8g [U-^{13}C]glucose/hr reproducibly resulted in outstanding signal-to-noise and excellent resolution of ^{13}C–^{13}C multiplets, allowing us to apply mathematical models of intermediary metabolism. Although informative NMR spectra can be obtained after an intravenous bolus without a continuous infusion [22], no metabolic steady-state is established under those conditions.

Systemic infusion of ^{13}C-enriched glucose provides glucose to other organs such as the liver and skeletal muscle that could, in principle, generate ^{13}C enriched glutamine that could be transferred via the circulation to the tumor. However, this is unlikely because we detected only very small amounts of ^{13}C-glutamine in the plasma of these patients. Furthermore, investigators have developed “chemical biopsy” methods to probe labeling patterns in hepatic glutamine and glutamate precisely because the human liver does not ordinarily export significant amounts of these amino acids [36]. We also considered the possibility that ^{13}C-labeled glutamate and/or glutamine was synthesized in the surrounding brain and then transferred to the tumor, exaggerating the ability of the tumor to oxidize glucose and produce these intermediates. Indeed, an earlier study used microdialysis to demonstrate that human brain releases glutamine synthesized *de novo* from ^{13}C-labeled nutrients into the interstitial space [37]. No release of ^{13}C-glutamate was detected in that study. However, examination of the tumor spectra in our study does not support a model in which the ^{13}C detected in tumor glutamate/glutamine originated from extracellular glutamine generated by adjacent tissue. If ^{13}C-glutamine entered the tumor from the interstitial space, and then was converted to glutamate, the fractional enrichment in glutamine would exceed that of glutamate. But we observed the opposite, as demonstrated by the differences in glutamate and glutamine multiplets, as illustrated in Fig. 1. Here the ratio of the singlet from natural abundance ^{13}C to the doublet from *de novo* synthesis is much higher in glutamine than

glutamate. This indicates a lower fractional enrichment in glutamine, and the pattern suggests that ^{13}C passes through the glutamate pool before reaching glutamine, rather than the opposite. This is most consistent with *de novo* synthesis of both glutamate and glutamine from glucose within the tumor.

All tumors consumed [U-^{13}C]glucose avidly, producing extensive ^{13}C–^{13}C coupling in numerous metabolites. Glucose metabolism through PDH and the TCA cycle was active in both primary and metastatic tumors. Thus, these tumors retained the enzymatic mechanisms to capture energy efficiently in the TCA cycle. This specific conclusion relies solely on qualitative analysis of the ^{13}C NMR spectra, and does not require any assumptions or mathematical modeling. The findings argue against the conventional perception of metabolism in ^{18}FDG-PET-positive tumors: that tumor glucose handling is dominated by production of the end products lactate and alanine. Although these two metabolites were observed in all tumors, their formation indicates that these human tumors *in situ* use both oxidative and non-oxidative metabolism concurrently [17, 38]. The data reinforce a recent reexamination of Warburg's work that stressed the complexity of tumor metabolism and the lack of evidence for suppression of respiration in most tumors, even those studied in Warburg's early experiments [39]. The observation of PDH activity in the tumors is particularly important because recent therapeutic efforts to modulate GBM metabolism *in vivo* have used agents intended to stimulate rather than suppress PDH [40].

Unexpectedly, we found that blood-borne glucose provided only a minority of the acetyl-CoA in the tumor TCA cycle. This finding contrasts with the normal brain, in which 95% of oxidative metabolism is supplied by glucose [41]. The results should be interpreted in view of two assumptions underlying ^{13}C NMR analysis. First, we assumed that the fractional enrichment of blood-borne glucose matched the enrichment in glucose available to the tumor. This seems reasonable since tumors tend to out-compete surrounding brain for ^{18}FDG-PET uptake, and because there was little change in the NMR spectra from tumor specimens obtained up to 30 minutes apart (data not shown). Second, the mathematical analysis requires that the tumor sample is homogeneous with respect to glucose metabolism. Although all tumor fragments contain small populations of non-malignant cells, the fragments used for ^{13}C NMR were carefully selected through pre-operative planning and imaging, stereotactic localization of fragments during the resection, and gross and histological examination of each sample to ensure that the tumor cellularity was as high as possible (see Materials and Methods), and that the resulting ^{13}C NMR spectrum reflected metabolism of *bona fide* tumor tissue. Thus, at the somewhat low level of resolution supported by this analysis (150–400 mg tumor fragments), every possible precaution was taken to maximize the homogeneity of the sample. With these assumptions in mind, the data imply that tumors oxidize other substrates in addition to blood-borne glucose. Metabolism of these alternative fuels, which could include glycogen, fatty acids, amino acids or organic acids, might be suitable therapeutic targets in human GBM because their utilization in the rest of the brain is expected to be minimal. Another possibility is that cytoplasmic lipid droplets contained in human and animal gliomas provide a dynamic reservoir of substrate for the production of acetyl-CoA in the mitochondria [42]. Future infusions with ^{13}C-labeled analogs of alternative nutrients will test these possibilities.

In addition to its role in producing energy, glucose also contributed to biosynthesis. Carbon from glucose was used to supply pools of the macromolecular precursors glutamate, glutamine, and glycine, which are required for protein and nucleic acid synthesis. Production of glutamine was particularly evident in GBMs, where the total ^{13}C NMR signal in glutamine exceeded the signal in corresponding glutamate carbons (Fig. 1d and Fig. 4e). Glycine is generated from the glycolytic intermediate 3-phosphoglycerate, which supplies carbon both to serine and glycine. We recently used *in vivo* ^{1}H MRS to identify a subset of

human GBMs with high intracellular glycine content [43]. Detection of glycine in the breast metastasis is of particular interest since phosphoglycerate dehydrogenase, an enzyme in the serine/glycine biosynthesis pathway, is commonly over-expressed in human breast adenocarcinoma, is amplified at the genomic level in a subset of these tumors, and is essential for tumor growth in a human breast cancer xenograft model [29]. Therefore the detection of glycine synthesis *in vivo* is likely to yield important information relevant to tumor growth.

Metabolism reflects many clinically important aspects of tumor biology, including proliferative state, response to chemotherapy and radiation, and possibly the effects of particular oncogenes. Thus it is striking that the metabolic activities of eleven independent tumors were so consistent. Further work is necessary to determine whether individual oncogenic mutations are associated with specific metabolic features that could be used to predict prognosis or to individualize therapy. For example, mutations in isocitrate dehydrogenase isoforms 1 and 2 are commonly found in low-grade gliomas and influence intermediary metabolism, including some of the pathways analyzed in this work [44–46]. There should be no major obstacles to extending this method to study low-grade gliomas and, importantly, to study the metabolism of other nutrients besides glucose.

CONCLUSIONS

In summary, these studies demonstrated that infusion of [U-^{13}C]glucose can be integrated easily into standard operating room procedures in patients undergoing surgical resection of high-grade gliomas and brain metastases. A simple protocol using an 8g bolus followed by an 8g/hr infusion of U-^{13}C]glucose produced a high steady-state enrichment of plasma glucose and excellent signal-to-noise in ^{13}C spectra of metabolites extracted from the tumor. Flux through PDH and turnover in the TCA cycle was active in all eleven tumors studied, indicating that oxidation in the mitochondria is a significant fate of glucose carbon. Glucose was also used to produce the nonessential amino acids glutamate, glutamine and glycine. ^{13}C NMR isotopomer analysis suggested that the tumors oxidized alternative substrates in the TCA cycle in addition to blood-borne glucose.

Supplementary Material

Refer to Web version on PubMed Central for supplementary material.

Acknowledgments

This work was supported by NIH grants RC 1CA146641, RR 02584 and R01 CA157996-01; a Damon-Runyon Clinical Investigator Award; CPRIT grants HIRP100437 and RP101243; and by a donation from the Kenny Can Foundation for Brain Cancer. We are grateful to Sarah McNeil for directing the ^{13}C-glucose infusion and collection of blood samples; Jessica Sudderth for measuring enrichment in glucose, glutamine and lactate; Chendong Yang and Kartik Rajagopalan for analyzing the cyst fluid for lactate and amino acids; and Christie Sheppard for managing the patient database.

ABBREVIATIONS

TCA	tricarboxylic acid cycle
^{18}FDG	2-^{18}fluoro-2-deoxyglucose
GBM	glioblastoma
GS	glutamine synthetase
HIF-1	hypoxia-inducible factor-1

IDH	isocitrate dehydrogenase
PDH	pyruvate dehydrogenase
PET	positron emission tomography
[U-^{13}C]glucose	uniformly-labeled glucose, i.e. D-glucose labeled in all six carbons with ^{13}C

REFERENCES

1. Hanahan D, Weinberg RA. Hallmarks of cancer: the next generation. Cell. 2011; 144:646–674. [PubMed: 21376230]
2. Warburg O. On the origin of cancer cells. Science. 1956; 123:309–314. [PubMed: 13298683]
3. Warburg O. On respiratory impairment in cancer cells. Science. 1956; 124:269–270. [PubMed: 13351639]
4. Vander Heiden MG, Cantley LC, Thompson CB. Understanding the Warburg effect: the metabolic requirements of cell proliferation. Science. 2009; 324:1029–1033. [PubMed: 19460998]
5. DeBerardinis RJ, Lum JJ, Hatzivassiliou G, Thompson CB. The biology of cancer: metabolic reprogramming fuels cell growth and proliferation. Cell Metab. 2008; 7:11–20. [PubMed: 18177721]
6. Dang CV. c-Myc target genes involved in cell growth, apoptosis, and metabolism. Mol Cell Biol. 1999; 19:1–11. [PubMed: 9858526]
7. Semenza GL. Regulation of cancer cell metabolism by hypoxia-inducible factor 1. Semin Cancer Biol. 2009; 19:12–16. [PubMed: 19114105]
8. Lu J, Sharma LK, Bai Y. Implications of mitochondrial DNA mutations and mitochondrial dysfunction in tumorigenesis. Cell Res. 2009; 19:802–815. [PubMed: 19532122]
9. Linehan WM, Srinivasan R, Schmidt LS. The genetic basis of kidney cancer: a metabolic disease. Nat Rev Urol. 2010; 7:277–285. [PubMed: 20448661]
10. Freisinger P, Futterer N, Lankes E, Gempel K, Berger TM, Spalinger J, Hoerbe A, Schwantes C, Lindner M, Santer R, Burdelski M, Schaefer H, Setzer B, Walker UA, Horvath R. Hepatocerebral mitochondrial DNA depletion syndrome caused by deoxyguanosine kinase (DGUOK) mutations. Arch Neurol. 2006; 63:1129–1134. [PubMed: 16908739]
11. Baysal BE, Ferrell RE, Willett-Brozick JE, Lawrence EC, Myssiorek D, Bosch A, van der Mey A, Taschner PE, Rubinstein WS, Myers EN, Richard CW 3rd, Cornelisse CJ, Devilee P, Devlin B. Mutations in SDHD, a mitochondrial complex II gene, in hereditary paraganglioma. Science. 2000; 287:848–851. [PubMed: 10657297]
12. Newsholme EA, Crabtree B, Ardawi MS. The role of high rates of glycolysis and glutamine utilization in rapidly dividing cells. Biosci Rep. 1985; 5:393–400. [PubMed: 3896338]
13. Bui T, Thompson CB. Cancer's sweet tooth. Cancer Cell. 2006; 9:419–420. [PubMed: 16766260]
14. Pfeiffer T, Schuster S, Bonhoeffer S. Cooperation and competition in the evolution of ATP-producing pathways. Science. 2001; 292:504–507. [PubMed: 11283355]
15. Gatenby RA, Gillies RJ. Why do cancers have high aerobic glycolysis? Nat Rev Cancer. 2004; 4:891–899. [PubMed: 15516961]
16. Hawkins RA, Coi Y, Huang SC, Messa C, Hoh CK, Phelps ME. Quantitating tumor glucose metabolism with FDG and PET. J Nucl Med. 1992; 33:339–344. [PubMed: 1740699]
17. DeBerardinis RJ, Mancuso A, Daikhin E, Nissim I, Yudkoff M, Wehrli S, Thompson CB. Beyond aerobic glycolysis: transformed cells can engage in glutamine metabolism that exceeds the requirement for protein and nucleotide synthesis. Proc Natl Acad Sci U S A. 2007; 104:19345–19350. [PubMed: 18032601]
18. Grassian AR, Metallo CM, Coloff JL, Stephanopoulos G, Brugge JS. Erk regulation of pyruvate dehydrogenase flux through PDK4 modulates cell proliferation. Genes Dev. 2011; 25:1716–1733. [PubMed: 21852536]

19. Fogal V, Richardson AD, Karmali PP, Scheffler IE, Smith JW, Ruoslahti E. Mitochondrial p32 protein is a critical regulator of tumor metabolism via maintenance of oxidative phosphorylation. Mol Cell Biol. 2010; 30:1303–1318. [PubMed: 20100866]
20. Wijnen JP, Van der Graaf M, Scheenen TW, Klomp DW, de Galan BE, Idema AL, Heerschap A. In vivo 13C magnetic resonance spectroscopy of a human brain tumor after application of 13C-1-enriched glucose. Magn Reson Imaging. 2010; 28:690–697. [PubMed: 20399584]
21. Petroff OA, Errante LD, Rothman DL, Kim JH, Spencer DD. Glutamate-glutamine cycling in the epileptic human hippocampus. Epilepsia. 2002; 43:703–710. [PubMed: 12102672]
22. Fan TW, Lane AN, Higashi RM, Farag MA, Gao H, Bousamra M, Miller DM. Altered regulation of metabolic pathways in human lung cancer discerned by (13)C stable isotope-resolved metabolomics (SIRM). Mol Cancer. 2009; 8:41. [PubMed: 19558692]
23. Patronas NJ, Di Chiro G, Kufta C, Bairamian D, Kornblith PL, Simon R, Larson SM. Prediction of survival in glioma patients by means of positron emission tomography. J Neurosurg. 1985; 62:816–822. [PubMed: 2987440]
24. Opstad KS, Ladroue C, Bell BA, Griffiths JR, Howe FA. Linear discriminant analysis of brain tumour (1)H MR spectra: a comparison of classification using whole spectra versus metabolite quantification. NMR Biomed. 2007; 20:763–770. [PubMed: 17326043]
25. Yang I, Aghi MK. New advances that enable identification of glioblastoma recurrence. Nat Rev Clin Oncol. 2009; 6:648–657. [PubMed: 19806145]
26. Fernandez CA, Des Rosiers C, Previs SF, David F, Brunengraber H. Correction of 13C mass isotopomer distributions for natural stable isotope abundance. J Mass Spectrom. 1996; 31:255–262. [PubMed: 8799277]
27. Malloy CR, Sherry AD, Jeffrey FM. Analysis of tricarboxylic acid cycle of the heart using 13C isotope isomers. Am J Physiol. 1990; 259:H987–H995. [PubMed: 1975735]
28. Malloy CR, Thompson JR, Jeffrey FM, Sherry AD. Contribution of exogenous substrates to acetyl coenzyme A: measurement by 13C NMR under non-steady-state conditions. Biochemistry. 1990; 29:6756–6761. [PubMed: 1975750]
29. Possemato R, Marks KM, Shaul YD, Pacold ME, Kim D, Birsoy K, Sethumadhavan S, Woo HK, Jang HG, Jha AK, Chen WW, Barrett FG, Stransky N, Tsun ZY, Cowley GS, Barretina J, Kalaany NY, Hsu PP, Ottina K, Chan AM, Yuan B, Garraway LA, Root DE, Mino-Kenudson M, Brachtel EF, Driggers EM, Sabatini DM. Functional genomics reveal that the serine synthesis pathway is essential in breast cancer. Nature. 2011; 476:346–350. [PubMed: 21760589]
30. Locasale JW, Grassian AR, Melman T, Lyssiotis CA, Mattaini KR, Bass AJ, Heffron G, Metallo CM, Muranen T, Sharfi H, Sasaki AT, Anastasiou D, Mullarky E, Vokes NI, Sasaki M, Beroukhim R, Stephanopoulos G, Ligon AH, Meyerson M, Richardson AL, Chin L, Wagner G, Asara JM, Brugge JS, Cantley LC, Vander Heiden MG. Phosphoglycerate dehydrogenase diverts glycolytic flux and contributes to oncogenesis. Nat Genet. 2011; 43:869–874. [PubMed: 21804546]
31. Burgess SC, Hausler N, Merritt M, Jeffrey FM, Storey C, Milde A, Koshy S, Lindner J, Magnuson MA, Malloy CR, Sherry AD. Impaired tricarboxylic acid cycle activity in mouse livers lacking cytosolic phosphoenolpyruvate carboxykinase. J Biol Chem. 2004; 279:48941–48949. [PubMed: 15347677]
32. Malloy CR, Sherry AD, Jeffrey FM. Evaluation of carbon flux and substrate selection through alternate pathways involving the citric acid cycle of the heart by 13C NMR spectroscopy. J Biol Chem. 1988; 263:6964–6971. [PubMed: 3284880]
33. Grobben B, De Deyn PP, Slegers H. Rat C6 glioma as experimental model system for the study of glioblastoma growth and invasion. Cell Tissue Res. 2002; 310:257–270. [PubMed: 12457224]
34. Bouzier AK, Quesson B, Valeins H, Canioni P, Merle M. [1-(13)C]glucose metabolism in the tumoral and nontumoral cerebral tissue of a glioma-bearing rat. J Neurochem. 1999; 72:2445–2455. [PubMed: 10349854]
35. Terpstra M, Gruetter R, High WB, Mescher M, DelaBarre L, Merkle H, Garwood M. Lactate turnover in rat glioma measured by in vivo nuclear magnetic resonance spectroscopy. Cancer Res. 1998; 58:5083–5088. [PubMed: 9823316]

36. Magnusson I, Schumann WC, Bartsch GE, Chandramouli V, Kumaran K, Wahren J, Landau BR. Noninvasive tracing of Krebs cycle metabolism in liver. J Biol Chem. 1991; 266:6975–6984. [PubMed: 2016309]
37. Gallagher CN, Carpenter KL, Grice P, Howe DJ, Mason A, Timofeev I, Menon DK, Kirkpatrick PJ, Pickard JD, Sutherland GR, Hutchinson PJ. The human brain utilizes lactate via the tricarboxylic acid cycle: a 13C-labelled microdialysis and high-resolution nuclear magnetic resonance study. Brain. 2009; 132:2839–2849. [PubMed: 19700417]
38. Sonveaux P, Végran F, Schroeder T, Wergin MC, Verrax J, Rabbani ZN, De Saedeleer CJ, Kennedy KM, Diepart C, Jordan BF, Kelley MJ, Gallez B, Wahl ML, Feron O, Dewhirst MW. Targeting lactate-fueled respiration selectively kills hypoxic tumor cells in mice. J Clin Invest. 2008; 118:3930–3942. [PubMed: 19033663]
39. Koppenol WH, Bounds PL, Dang CV. Otto Warburg's contributions to current concepts of cancer metabolism. Nat Rev Cancer. 2011; 11:325–337. [PubMed: 21508971]
40. Michelakis ED, Sutendra G, Dromparis P, Webster L, Haromy A, Niven E, Maguire C, Gammer TL, Mackey JR, Fulton D, Abdulkarim B, McMurtry MS, Petruk KC. Metabolic modulation of glioblastoma with dichloroacetate. Sci Transl Med. 2010; 2 31ra34.
41. Clarke, DD.; Sokoloff, L., editors. Basic Neurochemistry: Molecular, Cellular and Medical Aspects. Philadelphia: Lippincott-Raven; 1999.
42. Opstad KS, Griffiths JR, Bell BA, Howe FA. Apparent T(2) relaxation times of lipid and macromolecules: a study of high-grade tumor spectra. J Magn Reson Imaging. 2008; 27:178–184. [PubMed: 18058932]
43. Choi C, Ganji SK, DeBerardinis RJ, Dimitrov IE, Pascual JM, Bachoo R, Mickey BE, Malloy CR, Maher EA. Measurement of glycine in the human brain in vivo by (1) H-MRS at 3 T: application in brain tumors. Magn Reson Med. 2011; 66:609–618. [PubMed: 21394775]
44. Reitman ZJ, Jin G, Karoly ED, Spasojevic I, Yang J, Kinzler KW, He Y, Bigner DD, Vogelstein B, Yan H. Profiling the effects of isocitrate dehydrogenase 1 and 2 mutations on the cellular metabolome. Proc Natl Acad Sci U S A. 2011; 108:3270–3275. [PubMed: 21289278]
45. Yan H, Parsons DW, Jin G, McLendon R, Rasheed BA, Yuan W, Kos I, Batinic-Haberle I, Jones S, Riggins GJ, Friedman H, Friedman A, Reardon D, Herndon J, Kinzler KW, Velculescu VE, Vogelstein B, Bigner DD. IDH1 and IDH2 mutations in gliomas. N Engl J Med. 2009; 360:765–773. [PubMed: 19228619]
46. Dang L, White DW, Gross S, Bennett BD, Bittinger MA, Driggers EM, Fantin VR, Jang HG, Jin S, Keenan MC, Marks KM, Prins RM, Ward PS, Yen KE, Liau LM, Rabinowitz JD, Cantley LC, Thompson CB, Vander Heiden MG, Su SM. Cancer-associated IDH1 mutations produce 2-hydroxyglutarate. Nature. 2009; 462:739–744. [PubMed: 19935646]
47. Cheng T, Sudderth J, Yang C, Mullen AR, Jin ES, Matés JM, DeBerardinis RJ. Pyruvate carboxylase is required for glutamine-independent growth of tumor cells. Proc Natl Acad Sci U S A. 2011; 108:8674–8679. [PubMed: 21555572]

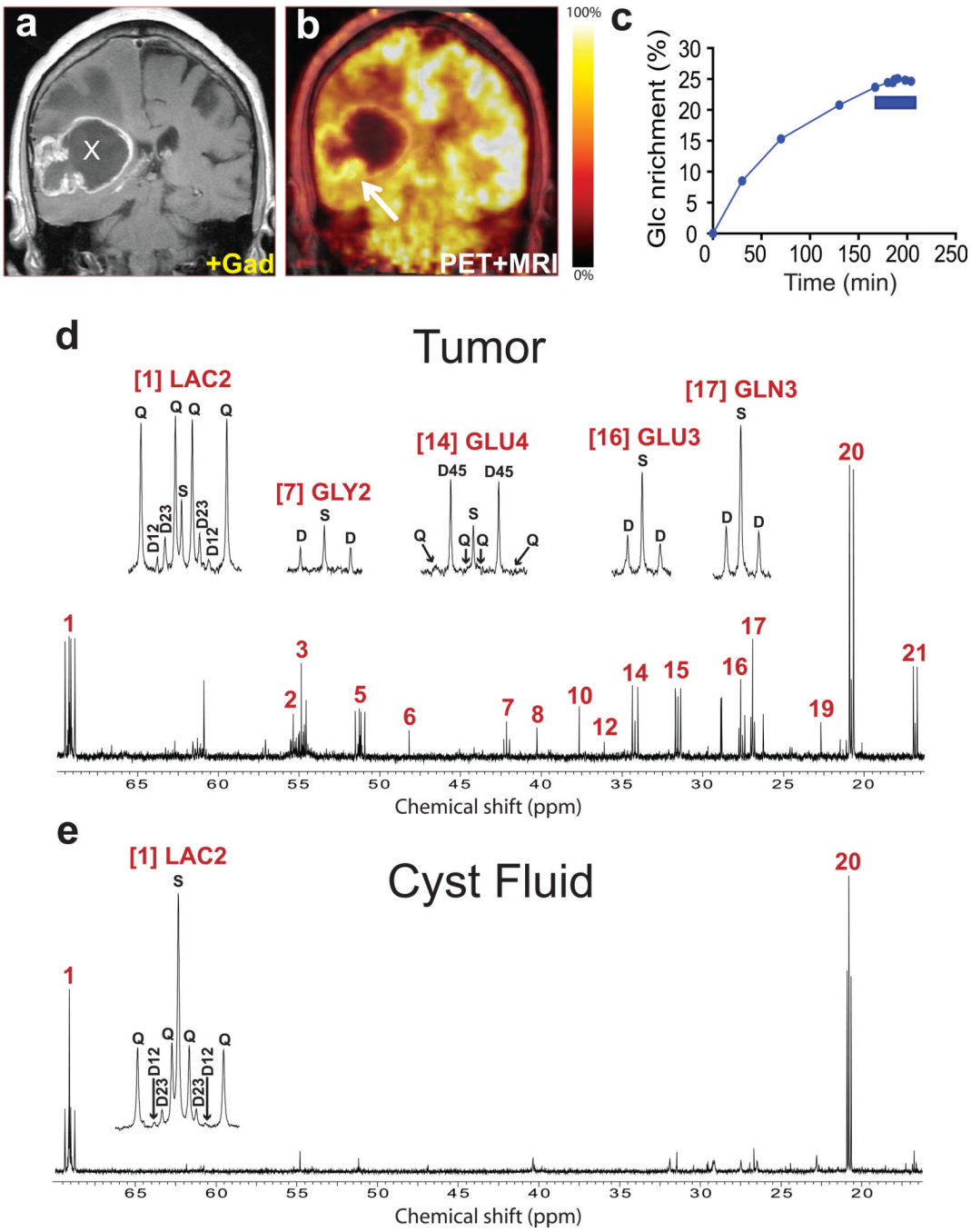

Fig. 1. Tumor glucose metabolism in a GBM patient infused with [U-^{13}C]glucose at 4 grams/hour

(a) Pre-operative T1-weighted post-gadolinium coronal image demonstrating a large right temporoparietal ring-enhancing mass lesion with a central cystic component (X) and surrounding edema. **(b)** ^{18}FDG-PET scan demonstrating uptake of ^{18}FDG along the tumor margin and inferior to the cyst (arrow). The expected high rate of cortical ^{18}FDG signal with reduced uptake in white matter is apparent in the left hemisphere. The blunted ^{18}FDG signal in the right hemisphere superior to the tumor is likely a consequence of tumor-associated edema. Histological analysis of the tumor sample revealed nearly 100% malignant cells. **(c)** Percent ^{13}C enrichment in plasma glucose (Glc) over the 200-minute infusion of

[U-^{13}C]glucose at 4g/hr. Enrichment is the fraction of plasma glucose that was uniformly labeled with ^{13}C. Tumor samples were collected during the final 35 minutes (blue bar). Proton-decoupled ^{13}C NMR spectra of **(d)** a tumor sample corresponding to the arrow in **(b)**; and **(e)** cyst fluid. The presence of multiplets at many of the highlighted resonances is the result of ^{13}C–^{13}C coupling. Assignments for all spectra throughout the paper: (1) Lactate C2; (2) Glutamate C2; (3) Glutamine C2; (4) Aspartate C2; (5) Alanine C2; (6) Taurine C1; (7) Glycine C2; (8) N-Acetylaspartate C3; (9) GABA C4; (10) Creatine C2; (11) Aspartate C3; (12) Taurine C2; (13) GABA C2; (14) Glutamate C4; (15) Glutamine C4; (16) Glutamate C3; (17) Glutamine C3; (18) GABA C3; (19) N-Acetylaspartate C6; (20), Lactate C3; (21) Alanine C3. The insets, from left to right, are Lactate C2; Glycine C2; Glutamate C4; and Glutamate and Glutamine C3. *Abbreviations:* S, singlet; D, doublet (e.g. D12, doublet arising from ^{13}C in carbons 1 and 2); Q, quartet (doublet of doublets).

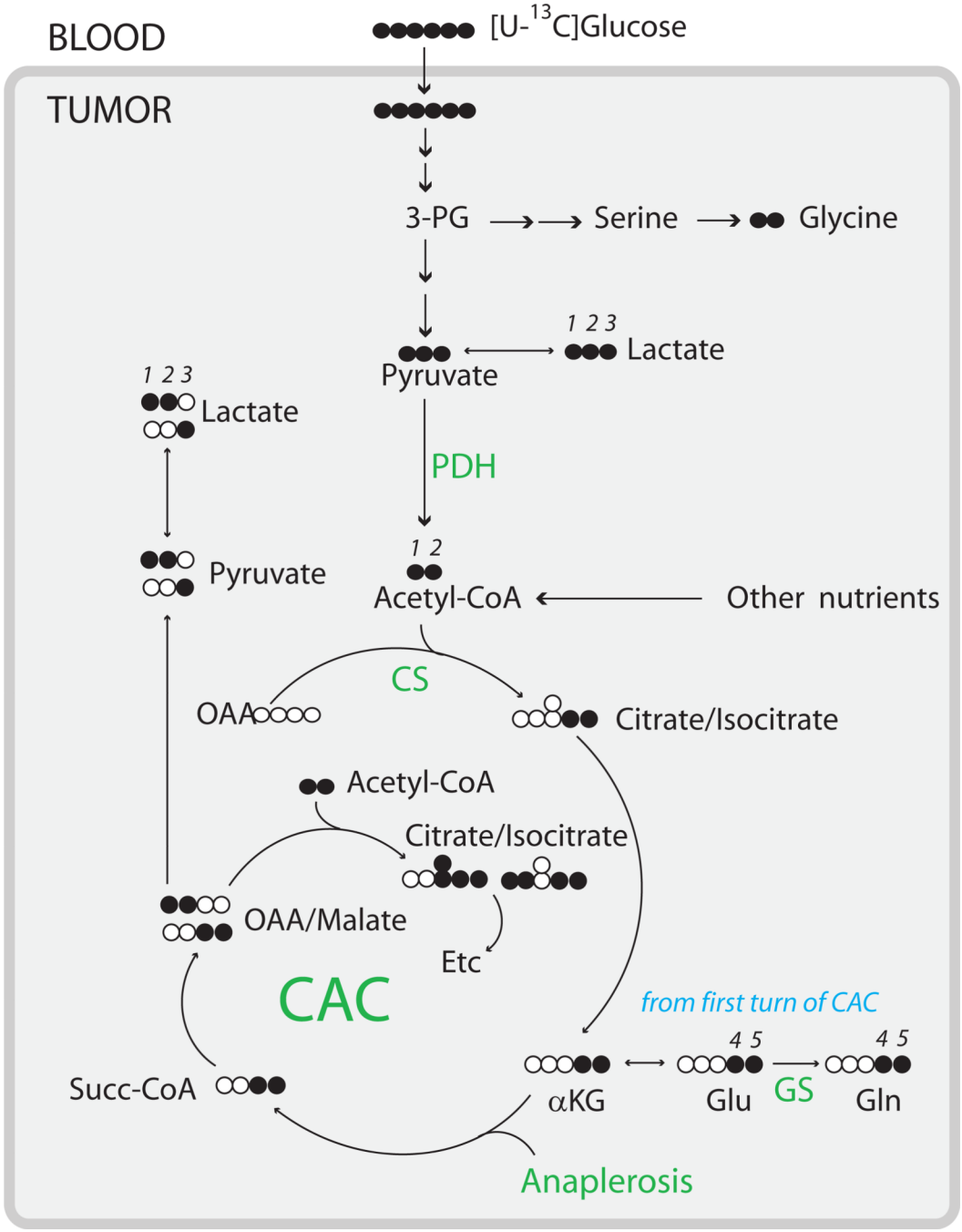

Fig. 2. Summary of glucose metabolism in human brain tumors *in vivo*

Filled symbols are ^{13}C, open symbols are ^{12}C. Numerals represent carbon positions within metabolites analyzed directly or indirectly by ^{13}C NMR in this study, and are included to aid in the interpretation of the spectra. Labeling beyond the first turn of the TCA cycle can be inferred from the ^{13}C distribution shown for citrate/isocitrate; additional detail is available [47]. Every pathway indicated in the diagram was observed in multiple tumors. The overall metabolic network involved metabolism of glucose to lactate through glycolysis and through more complex metabolic pathways involving part of the TCA cycle and/or the pentose phosphate pathway (data not shown). Pyruvate dehydrogenase (PDH), citrate synthase (CS), complete turnover of the TCA cycle, anaplerosis, and synthesis of glutamate and glutamine

from glucose were evident in all eleven tumors. *De novo* glycine synthesis was apparent in the astrocytoma, the metastatic breast tumor, and in 7 of 8 glioblastomas. GS, glutamine synthetase.

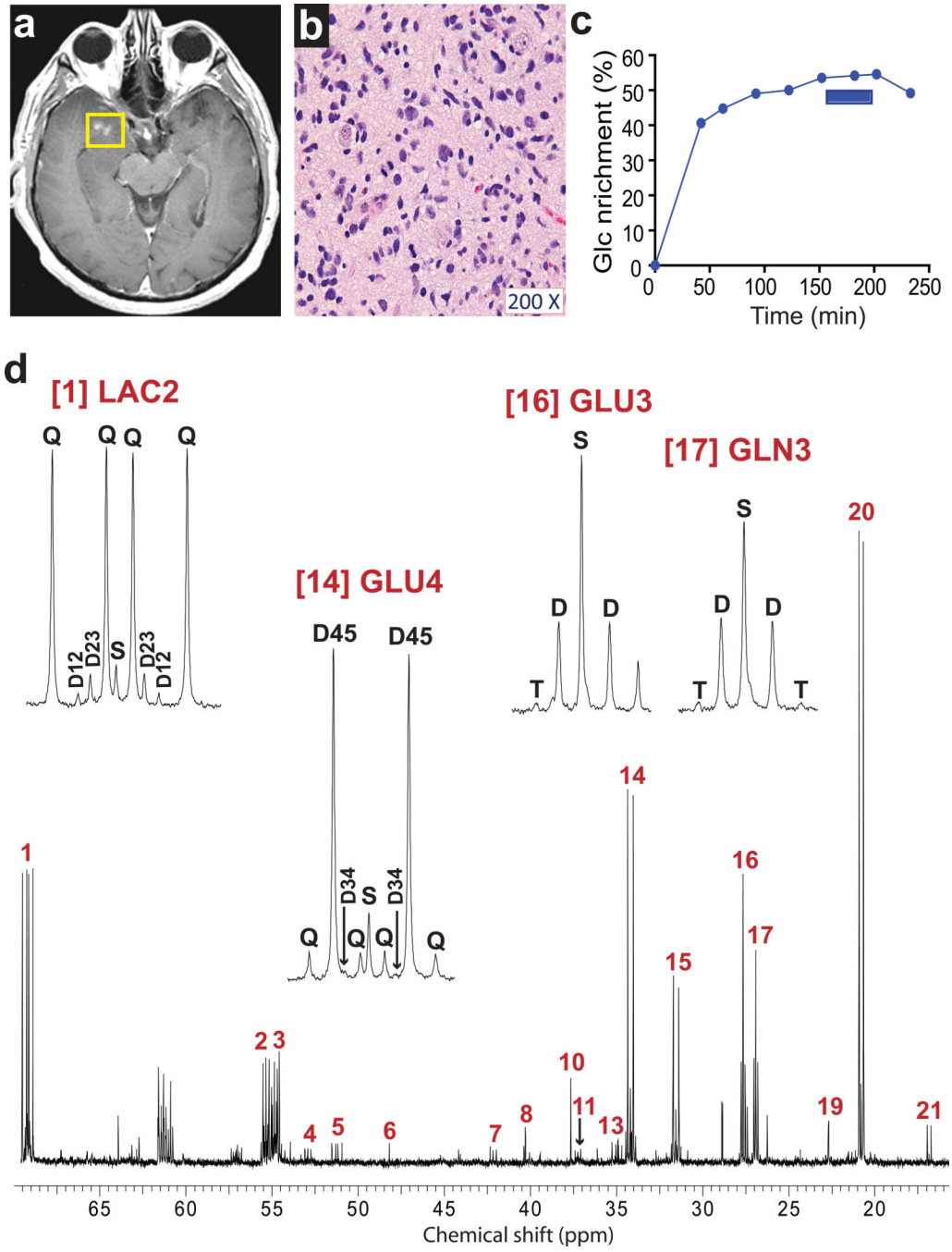

Fig. 3. Tumor glucose metabolism in a patient with WHO Grade III astrocytoma infused with [U-^{13}C]glucose at 8 grams/hour

(a) Pre-operative T1-weighted post-gadolinium axial image demonstrating nodular enhancement in the right temporal lobe. **(b)** Hematoxylin and eosin staining of a histological section prepared from the resected specimen. Cellularity: ~80% neoplastic nuclei and ~20% nuclei from nonmalignant cells (neurons, astrocytes, oligodendrocytes, and endothelial cells). **(c)** Time course of enrichment of plasma glucose (Glc). This patient received an 8g bolus of [U-^{13}C]glucose followed by an infusion of 8g/hr. The samples of tumor tissue were removed between 150 and 200 minutes (blue bar) and the infusion was discontinued after the last tumor sample was collected, 30 minutes prior to the final plasma sample. **(d)** Proton-

decoupled ^{13}C NMR spectrum of tumor tissue. *Abbreviation:* T, triplet due to enrichment in carbons 2, 3 and 4 of glutamate or glutamine. Assignments and other abbreviations are the same as in Fig. 1.

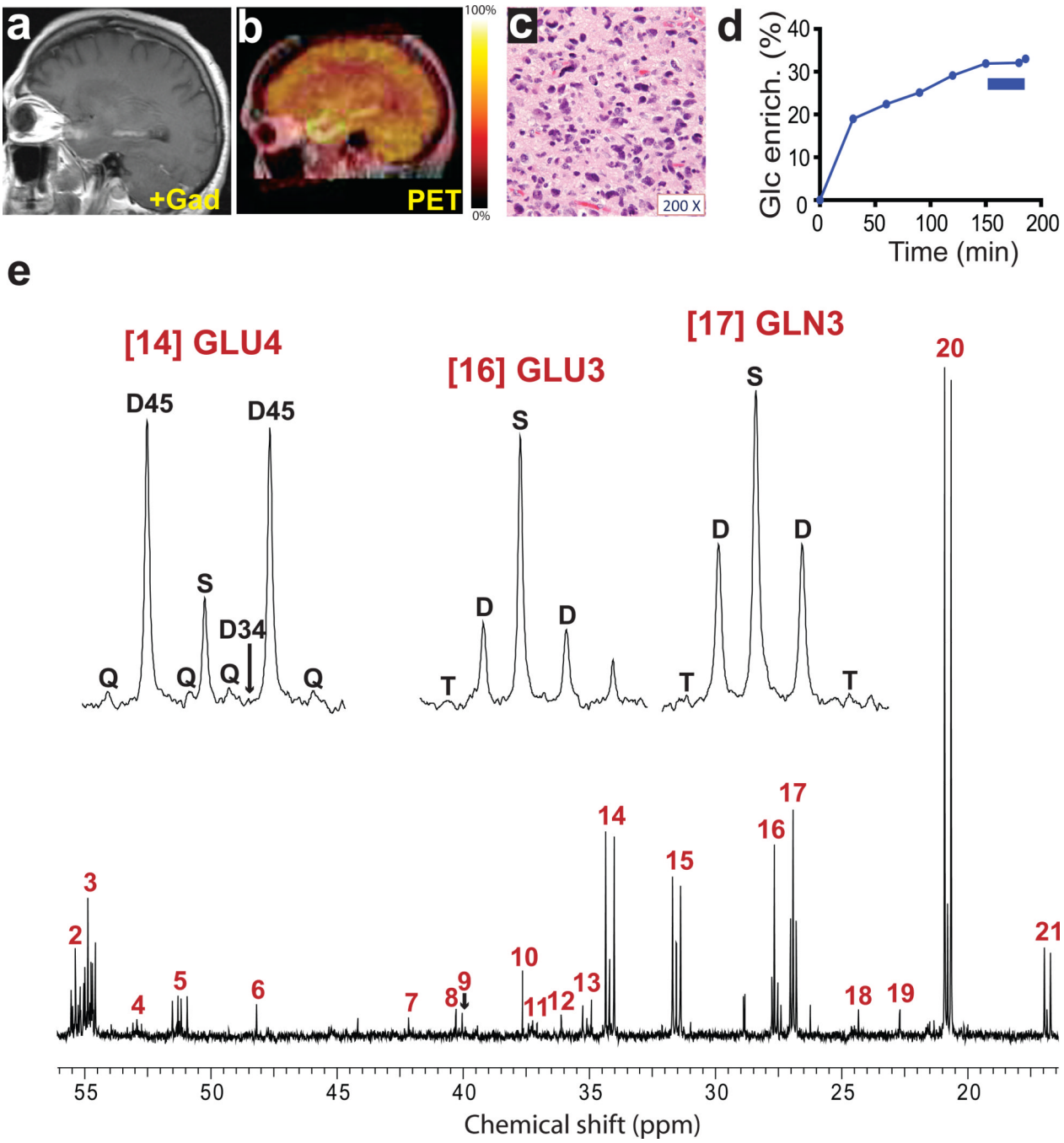

Fig. 4. Tumor glucose metabolism in a GBM patient infused with [U-^{13}C]glucose at 8 grams/hour

a, Pre-operative T1-weighted post-gadolinium sagittal image demonstrating an enhancing lesion in the left temporal lobe. **b,** ^{18}FDG-PET scan demonstrating uptake of ^{18}FDG in the region corresponding to T1 enhancement. **c,** Representative hematoxylin and eosin-stained section (200× magnification) of the tumor sample revealing features of GBM. Virtually 100% of the live cells in the sample were neoplastic. **d,** Percent ^{13}C enrichment in plasma glucose (Glc). This patient received an 8g bolus followed by an 8g/hr infusion of [U-^{13}C]-glucose. Note that this patient had steroid-induced hyperglycemia, and this resulted in a relatively low final enrichment in plasma glucose. The blue bar corresponds to removal of

the tumor samples. **e,** Proton-decoupled ^{13}C NMR spectrum of metabolites extracted from the tumor. Assignments and abbreviations are the same as in Figure 1.

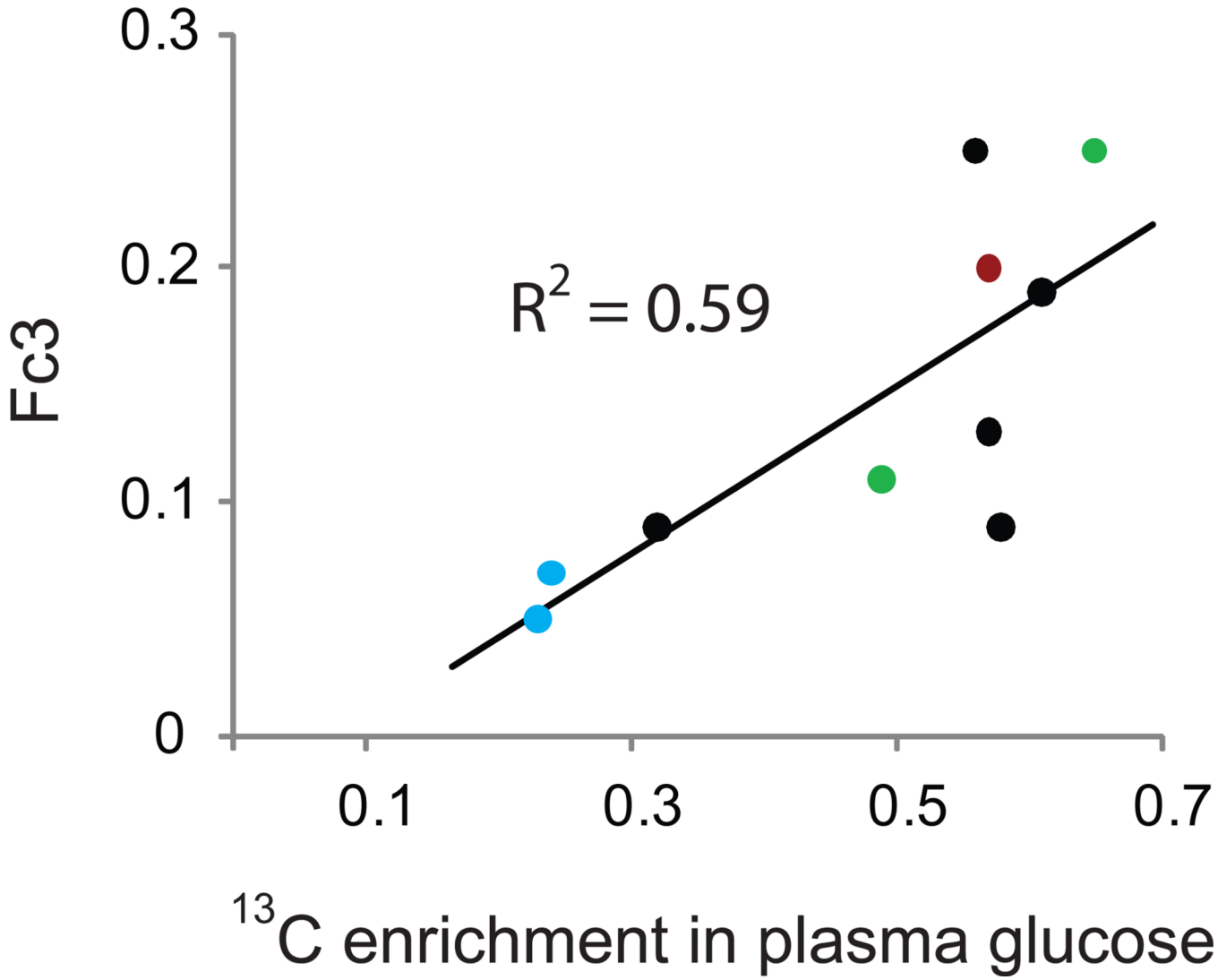

Fig. 5. Correlation between plasma glucose enrichment and content of [1,2-^{13}C]acetyl-CoA in tumor TCA cycle

^{13}C enrichment in plasma glucose near the time of tumor sampling was determined by mass spectrometry for each patient. This value was plotted against the value of Fc3 (i.e. the fraction of acetyl-CoA entering the TCA cycle that was ^{13}C-labeled on both carbons, [1,2-^{13}C]acetyl-CoA) determined from each tumor spectrum using a non-steady state analysis. Note that in every patient, ^{13}C enrichment in plasma glucose far exceeded Fc3. The blue symbols are from two of the glioblastoma patients analyzed using the 4 gram per hour infusion with [U-^{13}C]-glucose (Fc3 could not be calculated from the spectrum of the third patient infused on this protocol). The black symbols are from the five glioblastoma patients analyzed using the 8 gram bolus of [U-^{13}C]-glucose followed by the 8 gram per hour infusion. The red symbol is the patient with WHO Grade III astrocytoma and the green symbols are from the two patients with brain metastases.

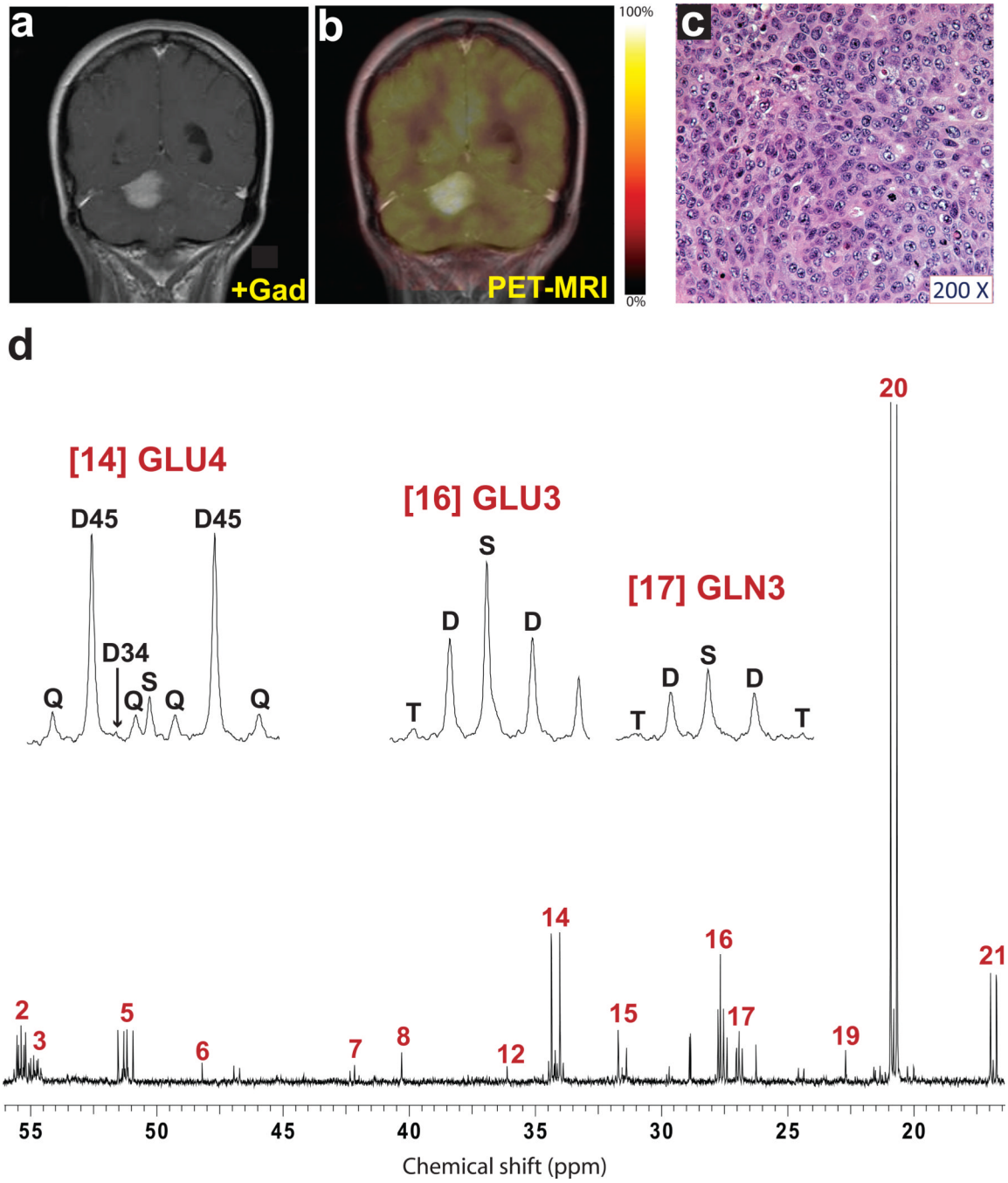

Fig. 6. Tumor glucose metabolism in a patient with metastatic breast cancer

Pre-operative imaging included **(a)** T1-weighted post-gadolinium coronal image demonstrating a large, solitary right cerebellar mass and **(b)** ^{18}FDG-PET scan demonstrating uptake of ^{18}FDG within the mass. **(c)** Hematoxylin and eosin staining of a histological section prepared from the resected specimen. Immunoperoxidase stains demonstrated expression of mammaglobin and BRST-2 (not shown) in neoplastic cells consistent with origin in the breast. This tumor was positive for the *HER-2* oncogene, and was negative for expression of the estrogen and progesterone receptors. Tumor cellularity was >99%. **(d)**

Proton-decoupled ^{13}C NMR spectrum of the tumor. Assignments and abbreviations are the same as in Fig. 1.

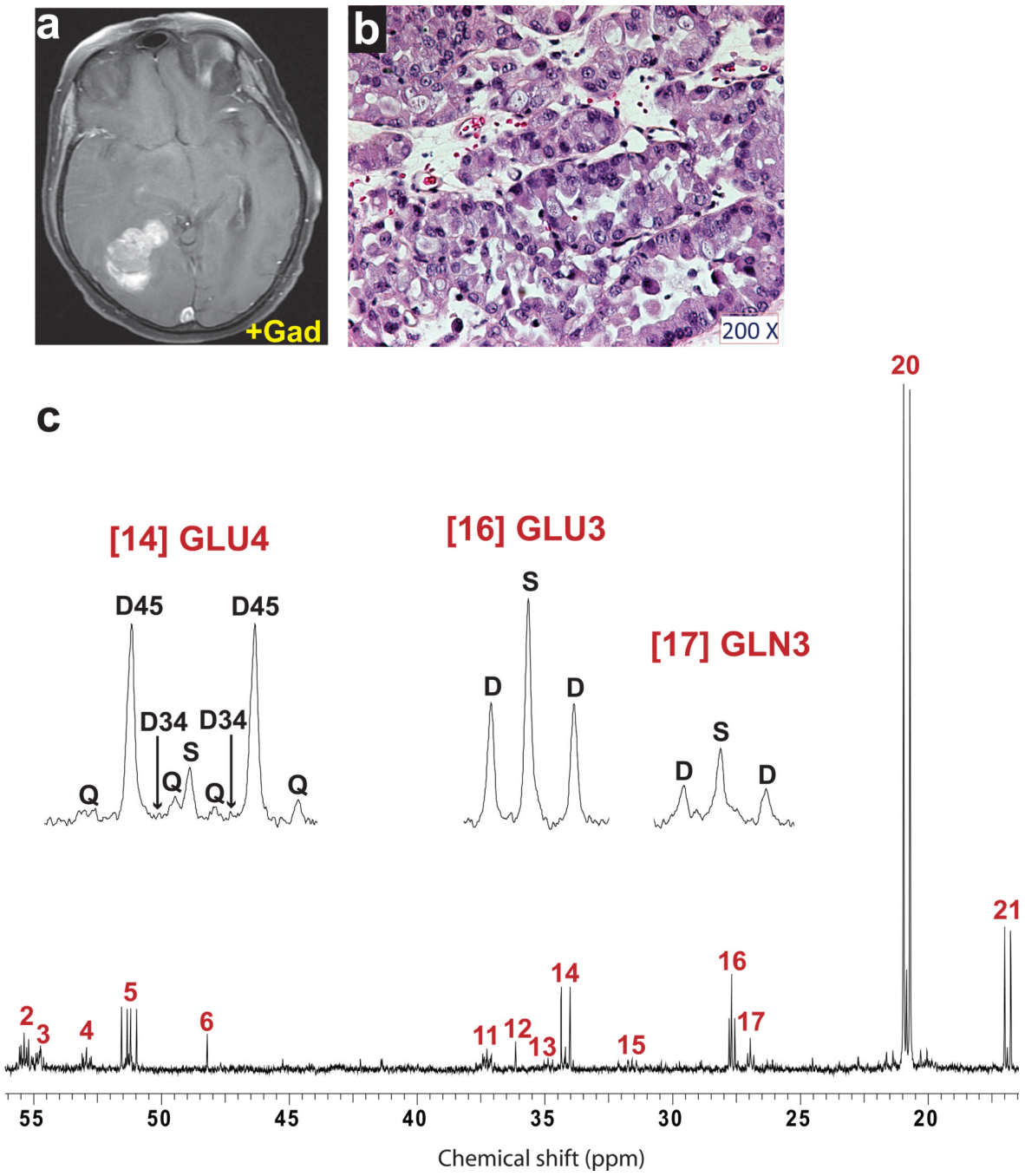

Fig. 7. Tumor glucose metabolism in a patient with metastatic non-small cell lung cancer

(a) Preoperative imaging included T1-weighted post-gadolinium axial image demonstrating a large right occipital mass. **(b)** Hematoxylin and eosin staining of a section prepared from the resected specimen. Immunoperoxidase stains demonstrated expression of thyroid transcription factor-1 (TTF-1) in neoplastic cells (not shown), consistent with origin in the lung. Tumor cellularity was ~95%. **(c)** Proton-decoupled ^{13}C NMR spectrum of the tumor. Assignments and abbreviations are the same as in Fig. 1.

Table 1

Summary of isotopomer analysis from eleven human brain tumors

Two types of infusions of [U-^{13}C]glucose were used: a 4g/hr infusion in patients 1–3, and an 8 g bolus followed by an 8 g/hr infusion in patients 4–11. In patient 3, no isotopmer analysis was performed because the resolution of the glutamate multiplets was poor. However, the spectral quality of eight patients infused with the Bolus + 8 g/hr protocol was sufficient for both non-steady state (NSS) and steady-state (SS) modeling. The mean and SD of metabolic parameters were calculated for the five GBM patients who received this type of infusion. Anaplerosis is defined as the anaplerotic flux relative to citrate synthase activity. Fc3, fraction of acetyl-CoA containing ^{13}C in both carbons ([1,2-^{13}C]acetyl-CoA).

Patient	Tumor type	Infusion protocol	Glucose m+6 (plasma)	NSS Fc3	SS Fc3	Anaplerosis
1	Glioblastoma	4 g/h	0.23	0.05		
2	Glioblastoma	4 g/h	0.24	0.07		
3	Glioblastoma	4 g/h	0.25	-		
5	Glioblastoma	Bolus + 8 g/h	0.32	0.09	0.06	1.63
6	Glioblastoma	Bolus + 8 g/h	0.58	0.09	0.08	1.80
7	Glioblastoma	Bolus + 8 g/h	0.57	0.13	0.08	0.94
8	Glioblastoma	Bolus + 8 g/h	0.61	0.19	0.17	0.94
9	Glioblastoma	Bolus + 8 g/h	0.56	0.25	0.19	0.94
		Mean	***0.53***	***0.15***	***0.11***	***1.25***
		SD	***0.12***	***0.07***	***0.06***	***0.43***
4	Grade III astrocytoma	Bolus + 8 g/h	0.57	0.20	0.21	0.84
10	Metastatic breast	Bolus + 8 g/h	0.65	0.25	0.22	0.58
11	Metastatic lung	Bolus + 8 g/h	0.49	0.11	0.05	1.81